Research Article

Yuejin Zhang, Mengqiu Ye, Juan Wang, Guanghui Li, Meiling Zhong, and Aiyun Zhan*

Modeling analysis of microenvironment of 3D cell mechanics based on machine vision

https://doi.org/10.1515/phys-2022-0013
received June 22, 2021; accepted November 15, 2021

Abstract: Aiming at the problem of poor construction accuracy of the cellular three-dimensional (3D) mechanical microenvironment, this article studies the cellular 3D mechanical microenvironment based on machine vision. The gelatin methacrylate microgel column was prepared by NIH/3T3 mouse fibroblast and precursor solution of gelatin methacrylate microgel. The gelatin methacrylate microgel array with magnetic end was adopted. The external magnetic field was used to load microgel array and build 3D mechanics microenvironment model. The deformed pictures of hydrogel under magnetic field were obtained by fluorescence microscope. The scanning electron microscope was used to characterize the pore structure of gelatin methacrylate hydrogel. The pictures obtained by machine vision method were used to calculate the deformed parameters of sample. The machine vision method adopted the discrete cosine transform for autofocus, and then used the image analysis and processing technology to identify and estimate the cell motion parameters. After getting the cell motion parameters, Comsol multiphysics (COMSOL) multiphysics multifield coupling finite element analysis software was adopted. The correlative numerical simulation method and gel deformed simulation method were used to obtain the mechanical changes of cells in the 3D mechanical microenvironment. Experimental results show that the modulus of gelatin methacrylate microgel is changed significantly during the tensile loading. The tensile strain and the cell spreading area are nonlinearly related. The increase in stiffness of the hydrogel substrate helps to promote cell proliferation to a certain extent.

Keywords: machine vision, cell, three-dimensional mechanics, microenvironment, modeling analysis

1 Introduction

Somatic cells are in a complex microenvironment. The dynamic balance of microenvironment is the basis of maintaining the normal behavior of cell. More researches show that mechanical stimulation signals exist widely in the cell microenvironment and play an important role in regulating the cell behavior. It is significant to carry out an interdisciplinary research on the three-dimensional (3D) mechanical microenvironment of cells and clarify the interaction between the mechanical stimulation signal and life activities [1]. For some practical engineering problems, it is very difficult to get the analytical solution due to the irregular geometrical properties of object and the nonlinear or nonuniform materials. The finite element method divides the research object into many elements at first and then researches the mechanical properties of these finite size elements. Finally, a set of algebraic equations, which takes the node displacement as unknown quantity, can be obtained. The existing calculation methods can be used to get the approximate value of unknown quantity at the node [2]. Its essence is to idealize the continuum with infinite degrees of freedom into the element geometry with finite degrees of freedom. According to the relationship between node force and displacement, the algebraic equations taking node displacement as unknown quantities are established, so that the problem is simplified into a structural problem, which is suitable for a numerical solution [3].

The stretch stress produced by cells in response period not only drives the cell migration and the construction of tissue morphology but also plays an important role in cell proliferation, apoptosis, and differentiation behavior [4]. The mechanical signals directly felt by somatic cells come from the surrounding extracellular matrix. The extracellular matrix consists of macromolecules such as collagen,

* **Corresponding author: Aiyun Zhan,** Department of Electronic Information, East China Jiaotong University, Nanchang 330013, China, e-mail: zhanaiyun84684@163.com
Yuejin Zhang, Mengqiu Ye, Juan Wang: Department of Electronic and Communication Engineering, East China Jiaotong University, Nanchang 330013, China
Guanghui Li: IoT Engineering Department, East China Jiaotong University, Nanchang 330013, China
Meiling Zhong: Department of Polymer Materials and Engineering, East China Jiaotong University, Nanchang 330013, China

laminin, elastin, proteoglycan, and glycoprotein. Its mechanical properties will directly influence the combination of adhesion plaque and ligands and the further regulation of cell adhesion, cytoskeleton assembly and dissociation, differentiation, and proliferation. This category belongs to passive dynamics stimulation. In the microenvironment, there are many kinds of stress stimulation, which belong to active mechanical stimulation.

During the 3D culture of cells by tissue engineering method, the cell mechanical microenvironment plays an important role in sequential studies. Only the stress of cells in 3D state is clear, and we can understand the process of cell formation well [5]. Therefore, the mechanical quantitative analysis for mechanical materials is very important. Martinez-Reina *et al.* researched the effects of cell nonuniformity and explained how to adjust the components and directions of basic multicellularunits in the process of reconstruction. Meanwhile, they predicted the arrangement of cell microstructure under different mechanical loading conditions, and the heterogeneity and mechanical properties of human femur under physiological loads [6]. A. Libchaber proposed that the increase of tensile stress led to the thinning of membrane bimolecular layer, and increased the membrane deformed energy related to channel formation and activation energy related to channel decomposition. In the nature, the force-sensitive ion channels played an important role in many physiological processes. When bacteria are subjected to low osmotic pressure, the force-sensitive ion channel acts as a safety valve. When sensing the rising turgidity on the cell, the channel will open the pore to reduce the turgidity and thus to prevent the cell from being dissolved [7]. Other mechanical stimulation sensors such as G protein-coupled receptors also have the ability to transmit mechanical signals.

According to the pixel distribution, brightness, and color information, the structure is transformed into digital signal [8]. The image system extracts the target features from these signals and controls the equipment actions by the discrimination results. Due to the high water-retaining property, controllable physical and chemical property, similar structure with extracellular matrix and good biocompatibility, the hydrogel can be used as a matrix material for simulating the cell microenvironment [9]. In this study, a finite element model was built based on machine vision technology. The construction, characterization, and application of the 3D mechanical microenvironment based on hydrogel were carried out. The modeling analysis of the 3D mechanical microenvironment of cells based on machine vision was researched. The machine vision was applied to the 3D mechanical microenvironment modeling and thus to improve the effectiveness of analysis [10–12].

2 Material methods

2.1 Experimental materials and methods

2.1.1 Experimental instruments

SensoPart V20C-CO-A2-C camera, CX-2000 ultraviolet cross linker made in UVP Company (USA), ShanShi SS-150 scanning electron microscope (SEM), NanoFocus laser confocal microscope, Olympus X81 fluorescence microscope made in Japan, Thermo Scientific cell incubator, Beckman flow cytometer, Beckman Coulter high-speed centrifuge, freeze desiccant, electric displacement platform made in Beijing Weina optical automation equipment Co., Ltd., IKA constant temperature magnetic force agitator, and baking oven of Tianjin Taist Instrument Co., Ltd.

2.1.2 Experimental materials

Extracellular matrix, photomask, polymethyl methacrylate (PMMA), microbead, acrylamide, methylenebisacrylamide, ammonium persulfate, gelatin, sodium alginate, high-glucose medium, trypsin, penicillin–streptomycin, fetal calf serum, double staining Annexin V-PE, paraformaldehyde, polyethylene glycol dimethacrylate, Duff's phosphate buffer solution, gelatin methacrylate, and antifade mounting medium.

2.1.3 Experimental method

The precursor solution of gelatin methacrylate hydrogel was placed in a special organic glass mold, and irradiated with 20–40 s at ultraviolet (UV). Then, they were cross-linked to form the hydrogel. The hydrogel was swelled for 24 h. The hydrogel was deformed under the action of magnetic field, and then the photographs of hydrogel with different degrees of deformation were obtained by fluorescence microscope. The deformed parameters of samples were obtained by analyzing the images obtained by machine vision. The pore structure of gelatin methacrylate hydrogel was characterized by SEM. The specific methods are as shown: first, the swelling equilibrium of gelatin methacrylate hydrogel substrate is continued for 24 h, and then the samples were processed with liquid nitrogen and placed in a freeze dryer. After freeze-drying for 8 h at –60°C, the samples are sprayed with gold on the surface until the samples are completely dehydrated. Moreover, the surface pore structure is characterized by SEM. The acceleration voltage is 15,000 V. The aperture information of SEM photo is analyzed by the method of machine vision.

2.1.3.1 Mechanical loading experiment

The special magnetic array was used to conduct the non-contact magnetic loading on the microgel column. To achieve different degrees of strain mechanical loading, the distance between the magnetic array and the magnetic end of microgel was controlled by the potential displacement platform.

2.1.3.2 Cell inoculation and cell culture

For the gelatin methacrylate microgel column, NIH/3T3 mouse fibroblast was used to mix the cell suspension with the same volume of precursor solution of gelatin methacrylate microgel. The final density of cells was 2×10^5 cell/mL. Then, UV was cross-linked to form microgel, which was washed with Dursler's phosphate buffer solution for three to five times and placed in the medium. The culture medium was replaced every 4 h on the first day. Subsequently, the culture medium was replaced every other day.

2.1.3.3 Construction of 3D mechanical microenvironment

To research the influence of different degrees of deformation on NIH/3E3 cells, the mechanical loading was conducted by external magnetic field based on the microgel array of gelatin methacrylate with magnetic end.

The photolithography was used to prepare the gelatin methacrylate microgel arrays. At first, the precursor solution of polyethylene glycol dimethacrylate and some magnetic beads were mixed evenly and dropped into the microporous organic glass mold. The designed magnet array was used to precisely control the position of magnetic beads in micropores, and cross-link the gel layer of polyethylene glycol dimethacrylate under the irradiation of UV. After that, the gelatin methacrylate precursor solution mixed with cells was added to the plexiglass mold, and the cover glass processed by TMSPMA (chemical silicone-containing acrylate monomer) was covered. The photomask was used to prepare the gel layer of gelatin methacrylate under the irradiation of UV. The diameters of gel layers of polyethylene glycol dimethacrylate and gelatin methacrylate are all 800 μm. Each microgel column consists of two parts: the magnetic terminal of polyethylene glycol dimethacrylate including magnetic beads and the gelatin methacrylate containing cells. Under the action of magnetic field, the magnetic end makes the gelatin methacrylate deforming. The mechanical stimulation is applied on cells in 3D microenvironment.

2.2 Machine vision imaging and recognition technology of cell in hydrogel environment

2.2.1 Calibration and automatic focus of machine vision in hydrogel environment

If the visual imaging is out of focus, the imaging quality will decline, which directly affects the subsequent application effect. Therefore, an autofocus technology is researched. In other words, based on, the automatic search of focusing position is realized by the focusing evaluation, so as to ensure that the vision system is imaged on the focal plane. In the frequency domain, the amount of image transformation and details are large during the focusing. Correspondingly, the number of high-frequency components is large. During the defocusing, the adjacent pixels in image influence each other [13], so the edge is fuzzy, and the number of details is small. Correspondingly, there are many low-frequency components. Therefore, the focus evaluation of machine vision imaging can be realized by the frequency component of image. Discrete cosine changes are performed on the $M \times N$ image. Thus, as equation (1):

$$D(k,l) = \frac{2}{\sqrt{MN}} c(k)c(l) \sum_{x=0}^{m-1} \sum_{y=0}^{n-1} \cos\frac{(2x+1)k\pi}{2M} \times \cos\frac{(2y+1)k\pi}{2N}. \tag{1}$$

In the above, x, $k = 0, 1, \cdots, M-1$, y, $l = 0, 1, \cdots, N-1$, and $f(x, y)$ are the pixel values of original image, and the coefficients $(c(k), c(l))$ are shown as equations (2) and (3):

$$c(k) = \begin{cases} 1/\sqrt{2}, & k = 0, \\ 1, & k = 1, 2, \cdots, m-1, \end{cases} \tag{2}$$

$$c(l) = \begin{cases} 1/\sqrt{2}, & l = 0, \\ 1, & l = 1, 2, \cdots, n-1. \end{cases} \tag{3}$$

After the discrete cosine transform, the coefficient matrix of different frequency components can be obtained. $D(0, 0)$ is the mean value of all pixel values of the original image (*i.e.*, the direct-current (DC) component of image). With the increase of the value of k and the value of l, $D(k, 0)$ and $D(0, l)$ represent the incremental size of the horizontal spatial frequency component and vertical

spatial frequency component. Therefore, the processing result of image after discrete cosine change mainly includes DC component and the cosine with frequency from low to high.

Construct a computer vision analysis system, load an optical microscope head in front of the CCD camera, prepare a methacrylic gelatin microgel column and place it on the microscope stage, collect cell images through the DH-CG300 video capture card (Zhongke Zhiyuan, Beijing, China), and connect the two value processing to obtain a grayscale image. The autofocus imaging projection model is shown in Figure 1.

To find the focusing point more accurately, we can establish the corresponding focusing evaluation function by increasing the proportion value of high-frequency component or the sensitivity to high frequency as equation (4):

$$D(k, l) = \sum_{x=0}^{X-1} \sum_{y=0}^{Y-1} \sqrt{(k^2 + l^2) D(k, l)^2}. \tag{4}$$

When focusing the position, we can see that the focus evaluation function has the maximum value. The focus evaluation function decreases with the increase of offsets between the lens and the focusing position. The focus evaluation can be realized by judging the value of focus evaluation function.

The focus evaluation function curve based on discrete cosine transform has only one peak value. The climbing method is used to search the peak value, so that the focusing position can be determined. The specific steps:

Step 1: set the focusing direction and moving step of lens, move the lens in a single direction, and calculate the value of focusing evaluation function;

Step 2: judge whether the function value increases progressively. If it decreases progressively, it is necessary to change the focus direction and set a smaller step length; and

Step 3: continue to move the lens and calculate its evaluation function value, jump to Step 2, and repeat the search until the focusing position is determined.

In the hydrogel environment, the cell imaging mainly consists of the direct reflection of cells, the scattered light in the reflected light of some cells, and the scattered light of light source.

The total light intensity $I_Z(x, y)$ from the cell to the imaging plane is shown as equation (5):

$$I_Z = I_\mathrm{d}(x, y) + I_\mathrm{s}(x, y) + I_\mathrm{b}(x, y). \tag{5}$$

Among them, $I_\mathrm{d}(x, y)$ and $I_\mathrm{s}(x, y)$ are the light intensity that the reflected light of cell directly and indirectly reaches the imaging surface. $I_\mathrm{b}(x, y)$ is the intensity of light scattered by the light source. According to Lambert–Beer experience, we can infer that the reflected light intensity and the distance between object and observer meet the exponential attenuation relationship. The light intensity transmission coefficient $t(x, y)$ can be expressed as formula (6):

$$t(x, y) = \mathrm{e}^{-\beta d(x,y)}, \tag{6}$$

where, β is the attenuation coefficient of medium and $d(x, y)$ denotes the distance from the corresponding point in image to the imaging surface in actual space. The direct reflected light of microparticles arriving at the imaging surface can be expressed as equation (7):

$$I_\mathrm{d}(x, y) = I_0(x, y)\mathrm{e}^{-\beta d(x,y)}, \tag{7}$$

$I_0(x, y)$ denotes the actual reflected light intensity at any point of microparticle.

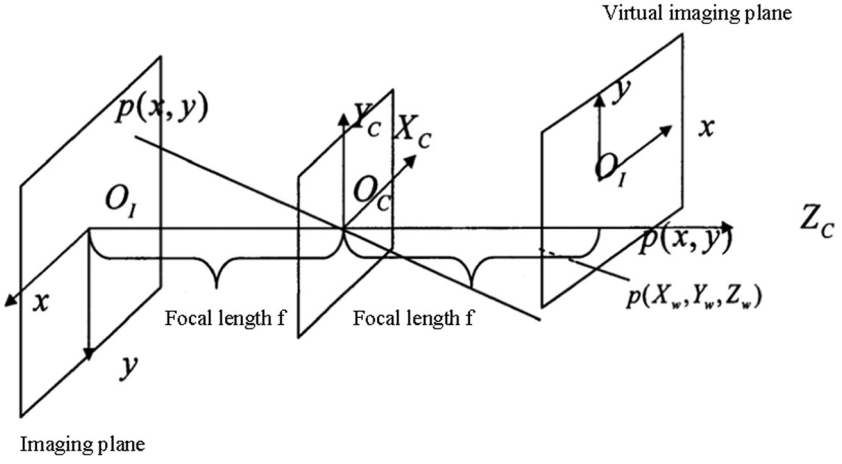

Figure 1: Autofocus imaging projection model.

The reflected light of cells and the scattered light of light source all reach the image surface after being refracted by the organics and suspension cells in hydrometer, but the refraction will increase the path of light propagation and cause the position shift [14]. Therefore, when they are superposed with the direct reflection light of target, it will lead to the imaging blur and the imaging quality reduction. To simplify the model, the two parts of the scattered light are collectively referred to as background light $A(x, y)$. Thus, the hydrogel imaging model can be obtained as equation (8):

$$I_r(x, y) = I_0(x, y)e^{-\beta d(x,y)} + (1 - e^{-\beta d(x,y)})A(x, y). \quad (8)$$

2.2.2 Identification and estimation of motion parameters of cells in hydrogel environment

The movement parameters of cell mainly include instantaneous velocity, average velocity, and acceleration in all directions [15,16]. It is only necessary to estimate the average velocity and speed variation rate of cells. The cell motion image recorded by machine vision system is discrete. Based on the difference method, the discrete cell position points and collection time interval are used to approximate the movement of microparticles [17] to achieve the estimation of cell motion parameters.

The acquisition speed of machine vision system is fixed. When the acquisition speed is M frames/s, the time interval Δt of any two consecutive frames is shown as equation (9):

$$\Delta t = t_i - t_{i-1} = 1/M, \quad (9)$$

t_i and t_{i-1} are two consecutive acquisition times.

Based on fuzzy mathematics theory to realize the positioning of the target particle center coordinates, use the canny edge operator and the membership function to calculate the membership of the nucleus center:

$$g > g_{TH}. \quad (10)$$

In the formula, g is the gray value of the center of the template, and g_{TH} is the set gray threshold. At this time, all pixels in the original image are given a central membership degree, and the point with the largest membership degree is selected as the cell center coordinate point.

When the center coordinates of the target microparticles in the image coordinate system are (x_i, y_i) and (x_{i+1}, y_{i+1}) in these two acquisition times, the corresponding displacement is shown as formula (11):

$$\begin{cases} d_x(i) = |x_i - x_{i+1}|g_x, \\ d_y(i) = |y_i - y_{i+1}|g_y, \end{cases} \quad (11)$$

d_x and d_y are the displacement of cells in the horizontal coordinates and vertical coordinates of any two consecutive images. g_x and g_y are the scale factors calibrated by the machine vision system.

According to the information of displacement and time, the cell velocity can be expressed as equation (12):

$$\begin{cases} v_x\left(\frac{x_i + x_{i+1}}{2}, \frac{y_i + y_{i+1}}{2}\right) = \frac{d_x(i)}{\Delta t}, \\ v_y\left(\frac{x_i + x_{i+1}}{2}, \frac{y_i + y_{i+1}}{2}\right) = \frac{d_y(i)}{\Delta t}, \end{cases} \quad (12)$$

where v_x and v_y are the components of cell velocity on axis X and axis Y at corresponding position, respectively.

After the velocity estimation is completed, the velocity change rate can be obtained by velocity estimation. Because the movement displacement of cell is relatively small, the velocity of cell at the previous position and the next position can be used to estimate the velocity change rate of cell at the current position [18], which is expressed as equation (13):

$$\begin{cases} \frac{dv_x\left(\frac{x_i + x_{i+1}}{2}, \frac{y_i + y_{i+1}}{2}\right)}{dt} \\ \quad = \frac{v_x\left(\frac{x_{i+1} + x_{i+2}}{2}, \frac{y_{i+1} + y_{i+2}}{2}\right) - v_x\left(\frac{x_{i-2} + x_{i-1}}{2}, \frac{y_{i-2} + y_{i-1}}{2}\right)}{\Delta t}, \\ \frac{dv_y\left(\frac{x_i + x_{i+1}}{2}, \frac{y_i + y_{i+1}}{2}\right)}{dt} \\ \quad = \frac{v_y\left(\frac{x_{i+1} + x_{i+2}}{2}, \frac{y_{i+1} + y_{i+2}}{2}\right) - v_y\left(\frac{x_{i-2} + x_{i-1}}{2}, \frac{y_{i-2} + y_{i-1}}{2}\right)}{\Delta t}, \end{cases} \quad (13)$$

2.3 Cellular 3D mechanical microenvironment modeling

The somatic cell can sense the stiffness of extracellular matrix, complex stress–strain stimulation, tensile and compressive stress, fluid shear stress, and so on. For muscle, connective tissue, lung, bladder, and other soft-tissue organs, the tensile mechanical stimulation is more common [19]. It is necessary to construct the tensile stress–strain microenvironment and research the influence of different tensile stress–strain stimulation on the cell behavior. At present, most of the construction systems mainly use the mechanics research to study cell response by stretching and loading cell basement (such as hydrogel, polymer film, and polydimethylsiloxane [PDMS]).

2.3.1 Numerical simulation method of magnetic field

COMSOL multiphysics multifield coupling finite element analysis software is used to simulate the deformation of hydrogel samples in magnetic field by combining solid mechanics module and magnetic field module. The deformed process of hydrogel under external load mainly includes two stages. The first one is the short-range movement between molecules. In this process, only the shape and properties of hydrogel was changed, but the volume will not be changed. The second is the long-range movement of water molecules. During this process, the volume of hydrogel remained unchanged, and the hydrogel was regarded as an elastic material. This is mainly due to the long molecular chain of hydrogel. In addition, the molecular chain is highly twisted and curled. Under stretching load, the molecular chain is expanded to the flat state [20]. Therefore, the hydrogel can withstand larger elastic deformation. The hydrogel almost does not cause deformation under hydrostatic pressure. In general, it is considered as incompressible material, and its Poisson's ratio is generally between 0.3 and 0.5. Based on the theory of continuous medium, the stress–strain curve is measured by experiment, and the strain energy function of material is obtained by fitting. The stress–strain curve is generally divided into four stages: elastic stage, yield stage, strengthening stage, and local deformation.

In the COMSOL software (Stockholm, Sweden), select the 3D simulated magnetic field, select the steady-state problem interface, and define the material properties to form a union.

The formula of material strain energy function is shown as equations (14) and (15):

$$W(I_1) = \frac{\mu}{2}(I_1 - 3), \tag{14}$$

$$\mu = E/2(1 + \nu). \tag{15}$$

In the above formulas, I_1 is the first principal invariant of Green strain tensor, μ denotes the shear modulus of hydrogel sample, E denotes the tensile modulus of hydrogel sample, and ν denotes the Poisson's ratio of hydrogel sample.

In the hydrogel environment, cell imaging is mainly composed of direct reflection of cells, scattered light in part of the reflected light of cells, and scattered light from a light source. Through the machine vision technology, the imaging clarity and image quality are improved, and the imaging model of the hydrogel is obtained. The simulation of static magnetic field around the permanent magnet is realized in the field current less module of COMSOL. The experimental environment is the room temperature and the external temperature is 300 K. The absolute environmental pressure is 1 atm. The steady-state equation of magneto static field around permanent magnet is shown as equations (16) and (17):

$$\nabla \cdot B = 0, \tag{16}$$

$$-\nabla \cdot (\mu_0 \nabla V_{\mathrm{m}} - \mu_0 M_0) = 0. \tag{17}$$

The magnetization direction is along the long axis of magnet. The distribution of magnetic field intensity around the permanent magnet can be obtained by steady-state solution. The formula to calculate the magnetic field force of magnetic bead in magnetic field is shown as equation (18):

$$\overrightarrow{F} = \int_A \mu_0^{-1} M_{\mathrm{sat}} \overrightarrow{\nabla B}(\overrightarrow{x}) \mathrm{d}A. \tag{18}$$

In the above formula, V_{m} denotes the scalar magnetic potential, B denotes the magnetic induction strength, M_0 denotes the magnetization strength, A denotes surface area of magnetic bead, μ_0 denotes the absolute permeability, M_{sat} denotes the saturation magnetization value of magnetic bead, and $\overrightarrow{\nabla B}$ denotes the gradient distribution of magnetic field strength.

The corresponding geometric model is built in COMSOL software. The sample boundary conditions are set under the solid mechanics module. The top of hydrogel sample is fixed constraint, and the bottom is subjected to magnetic force. At the interface, the magnetic force expression is calculated by inputting the current less module of magnetic field, and then the coupling between magnetic field and mechanical module is achieved to simulate the deformed process of hydrogel sample under the magnetic field.

2.3.2 Deformed simulation of hydrogel

For the construction of the 3D gradient mechanical microenvironment, the shapes of different hydrogel are related to the surface strain distribution during the stretching process. For the trapezoidal hydrogel, the surface strain distribution during the stretching process is shown as equation (19)

$$\varepsilon = \frac{\varepsilon_0}{1 - k\frac{x}{H}}. \tag{19}$$

In the above, H denotes the height of trapezium, k denotes the slope of gradient distribution function, and ε_0 denotes the minimum strain on the surface of trapezoidal hydrogel.

According to the theory of linear elasticity, if the hydrogel is very thin and the strain in the direction of thickness of hydrogel is very small, the hydrogel strain should meet equation (20):

$$\varepsilon = \frac{\sigma}{E} = \frac{1}{E}\frac{F}{lh}. \tag{20}$$

In the above, F denotes the tensile load, E denotes the tensile modulus of hydrogel sample, and l denotes the trapezoidal width.

Equation (20) is substituted into equation (19), so that the hydrogel shape function can be expressed as equation (21):

$$\frac{l}{l_1} = 1 - k\frac{x}{H}. \tag{21}$$

Similarly, different strain distributions can be designed [21], so that the corresponding hydrogel shape functions can be obtained. Meanwhile, the strain distributions of linear, parabolic, and exponential relations are designed respectively. The formula is shown as equations (22)–(24):

$$\varepsilon_1 = \varepsilon_0\left(1 + k\frac{x}{H}\right), \tag{22}$$

$$\varepsilon_2 = \varepsilon_0\left[1 + k\left(\frac{x}{H}\right)^2\right], \tag{23}$$

$$\varepsilon_3 = \varepsilon_0 \exp\left(k\frac{x}{H}\right). \tag{24}$$

The corresponding shape function is shown as equations (25)–(27):

$$\frac{l}{l_1} = 1\Big/\left(1 + k\frac{x}{H}\right), \tag{25}$$

$$\frac{l}{l_2} = 1\Big/\left[1 + k\left(\frac{x}{H}\right)^2\right], \tag{26}$$

$$\frac{l}{l_3} = 1/\exp\left(k\frac{x}{H}\right). \tag{27}$$

Based on the above process, the correlation simulation of gel deformation and magnetic field in the 3D mechanical microenvironment is realized.

3 Experimental results

In this experiment, the concentration of polyethylene glycol dimethacrylate is high (12.5% w/v). The purpose is to avoid deformation as much as possible under the magnetic effect. After applying a magnetic load to it, we can see that the maximum strain of magnetic end of polyethylene glycol dimethacrylate under magnetic field is less than 3%. The gelatin methacrylate at 5% (w/v) concentration, 10% (w/v) concentration, and 15% (w/v) concentration is selected. The deformed behavior of gelatin methacrylate microgel column under magnetic field was characterized by the proposed method. Because the microgel column has two layers, it is easy to lead to the stress concentration at the joint of polyethylene glycol dimethacrylate and gelatin methacrylate gel layers. Meanwhile, it tends to fracture during tensile loading. Before cross-linking of gelatin methacrylate, it should be laid for a period of time, then cross-linking UV. The purpose is to diffuse the gelatin methacrylate solution to the gel network of polyethylene glycol dimethacrylate and enhance the strength of the junction of gel layers through the interpenetrating network. The pore structure of the gelatin methacrylate hydrogel was characterized by scanning electron microscopy, and the SEM image is shown in Figure 2.

According to Figure 2, it can be seen that the methacrylic acid gelatin hydrogel is porous with uniform pore size and smooth cross section. The scanning electron micrograph of the local morphology of the composite gel particles is shown in Figure 3.

The influence of standing time on the maximum strain of microcolumn gel of gelatin methacrylate is shown in Figure 4.

As can be seen in Figure 1, the longer the standing time, the greater the maximum strain of the methacrylic gelatin microcolumn gel. The influence of UV illumination time on the maximum strain of microcolumn gel of gelatin methacrylate is shown in Figure 5.

The results show that the maximum strain of methacrylate gelatin layer can reach 180%. By analyzing the influence of different standing time and UV light time on the maximum strain of microgel column, we optimized the technological parameters. Finally, we determined that the standing time was 12–16 min and the UV irradiation time was 30 s. The methacrylate gel layer has the highest strain at this time.

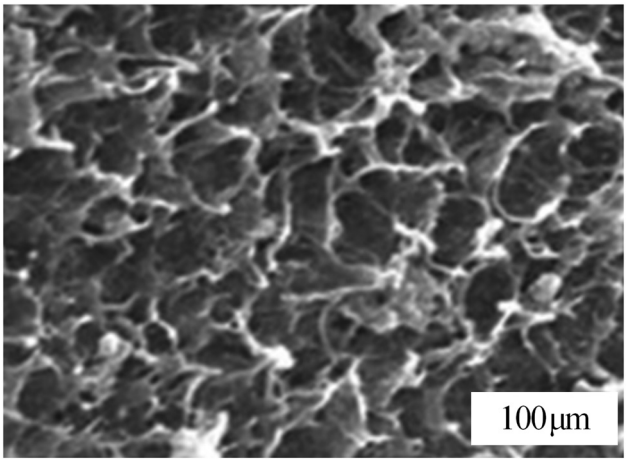

Figure 2: Pore structure of gelatin methacrylate hydrogel.

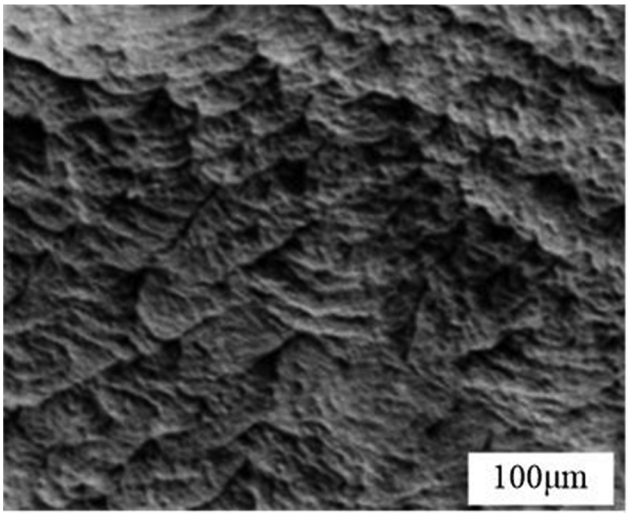

Figure 3: Scanning electron micrograph of local morphology of composite gel particles.

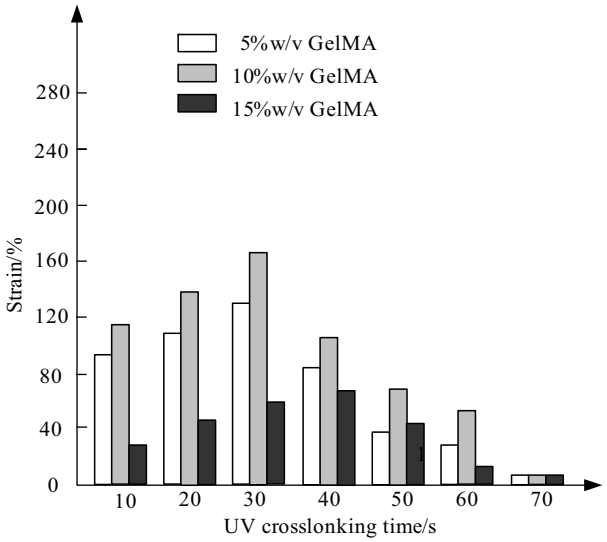

Figure 5: Effect of UV light time on the maximum strain of microgel columns.

Combined with magnetic loading experiment and finite element analysis, we obtained the stress–strain relationship of different proportions of gel layers (see Figure 6):

The mechanical relationship between different gelatin methacrylate microgel columns is shown in Figure 3. It is approximately linear within the range of 210% strain. We can see that the modulus of gelatin methacrylate microgel does not change significantly during tensile loading. Therefore, the influence of matrix stiffness and tensile strain on the cell behavior can be researched in the 3D mechanical microenvironment. After the finite element calculation, we can see that the tensile modulus at gel layer of gelatin methacrylate of 5, 10, and 15% w/v is about 2, 6, and 11 kPa, respectively. When the concentration of methacrylic gelatin gel layer is 15% w/v, its tensile modulus is the largest.

The influence of the large deformation of matrix on the cell behavior in the 3D mechanical microenvironment was researched. Based on the matrix stiffness and tensile strain in the 3D mechanical microenvironment, the NIH/3T3 cell spreading behavior was studied.

The influence of the cell remodeling on the stiffness of gel layer of methacrylate gelatin was investigated.

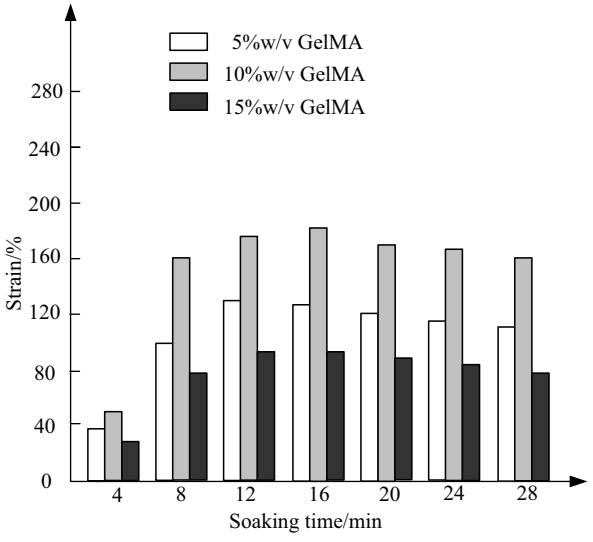

Figure 4: Effect of standing time on the maximum strain of microgel columns.

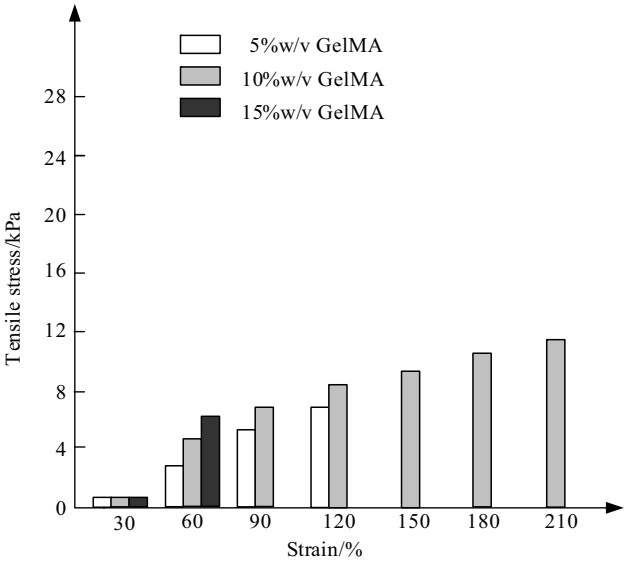

Figure 6: Stress–strain relationship of GelMA gel layers with different proportions.

Considering 6 kPa microgel as an example, the influence of culture time on the gel stiffness of methacrylate gelatin is shown in Figure 7.

Figure 7 shows that after culturing for 5 days, there was no significant change in the stiffness of methacrylate gelatin layer, indicating that the degradation of extracellular matrix by cells did not affect the stiffness of gel within 5 days.

The relationship between the matrix stiffness and tensile strain and the cell spreading behavior is shown in Figure 8.

The experimental results in Figure 8 show that when the tensile strain is not applied, the spreading behavior of cells in the gel is inhibited with the increase of gel stiffness. The reason is that with the increase of stiffness, the network structure in the gel becomes denser, which limits the cell spreading space to a certain extent. For gelatin methacrylate microgel with different stiffness, the tensile strain promotes cell spreading in gel, and it tends to be stable on the third day of culture, so there is a nonlinear relationship between tensile strain and cell spreading area.

According to the physiological load, 1,000 με constrained load and 2,000 με constrained load were applied to the top of cell model, respectively. All units on the bottom of cell model were set as the fixed constraints. The Poisson's ratio is 0.3.

Because the cell structure is too complex, the numbers of cell meshes are different when the finite element model is built. The average number of elements in 1,000 με group is about 470,000–480,000. Many elemental strains are far less than the applied apparent strain. Eighty percent of the elemental strains are less than 800 με. The

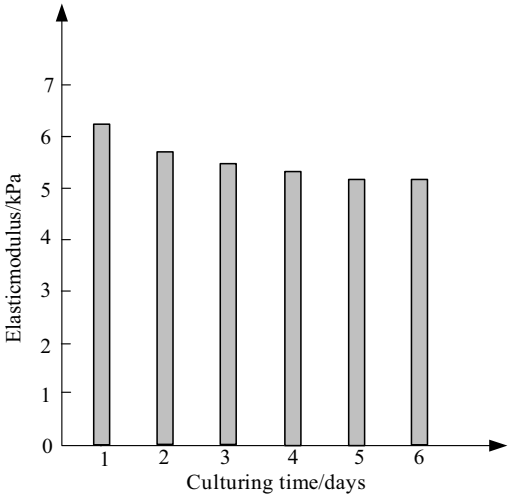

Figure 7: Effect of culture time on GelMA gel stiffness.

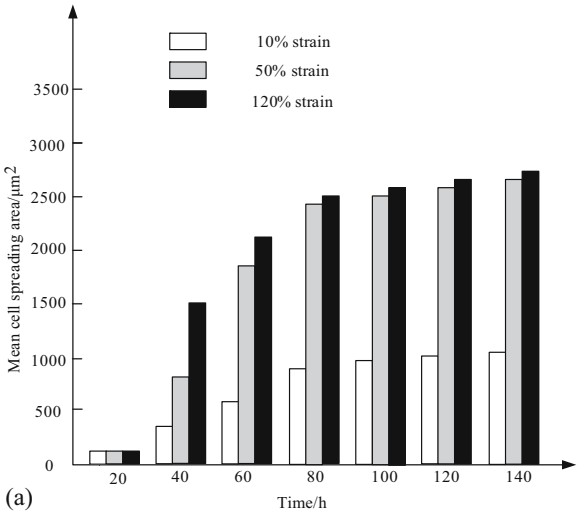

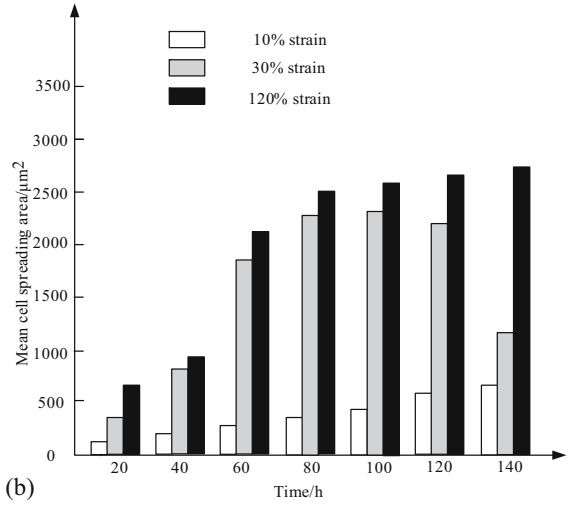

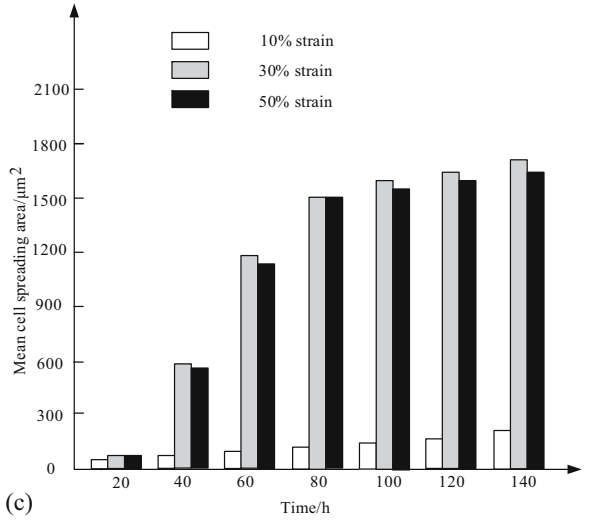

Figure 8: (a) Quantitative relationship between cell spreading area and culture time at 2 kPa, (b) quantitative relationship between cell spreading area and culture time at 6 kPa, and (c) quantitative relationship between cell spreading area and culture time at 10 kPa.

Table 1: Internal strain distribution of cells when 1,000 με apparent strain is applied

Strain (ε)	Number of elements	Percentage (%)
1.0×10^{-4}	17	0.0036
2.0×10^{-3}	10,205	2.18
1.5×10^{-3}	10,801	2.36
1.0×10^{-3}	31,033	6.77
9.0×10^{-4}	11,305	2.47
8.0×10^{-4}	14,405	3.14
7.0×10^{-4}	20,038	4.37
6.0×10^{-4}	25,065	5.47
5.0×10^{-4}	32,284	7.04
4.0×10^{-4}	42,288	9.22
3.0×10^{-4}	55,634	12.13
2.0×10^{-4}	69,845	15.23
$<2.0 \times 10^{-4}$	145,856	31.81

dependence decreases with the increase of strain value. Some phenomena show the stress concentration. The strain value is more than 1,000 με, and the maximum value is 1,300,000 με. The results and the strain distribution inside the cell are shown in Table 1.

Based on the finite element analysis method, the strain distribution of cells under 1,000 με and 2,000 με apparent loads in physiological range was obtained. The strain value was far less than the apparent load. The main mechanical effects of cells in the 3D culture were obtained. The mechanical response of most units in cell is far less than the apparent strain that the tissue can bear, so it has enough bearing strength and antifatigue strength. Tables 1 and 2 show that the cell proliferation was not affected by mechanical loading.

Table 2: Internal strain distribution of cells when 2,000 με apparent strain is applied

Strain (ε)	Number of elements	Percentage (%)
1.00×10^{-4}	21	0.00397
2.00×10^{-3}	12,645	2.39
1.50×10^{-3}	13,546	2.56
1.00×10^{-3}	38,456	7.27
9.00×10^{-4}	12,364	2.34
8.00×10^{-4}	15,564	2.94
7.00×10^{-4}	22,254	4.21
6.00×10^{-4}	27,054	5.11
5.00×10^{-4}	34,685	6.56
4.00×10^{-4}	44,685	8.44
3.00×10^{-4}	57,465	10.86
2.00×10^{-4}	71,685	13.55
$<2.0 \times 10^{-4}$	178,654	33.77

4 Discussions

This article uses the machine vision and cell 3D mechanical microenvironment modeling to effectively analyze the cell behavior. Considering hydrogel as the research object, an experimental system was built to characterize the mechanical properties of hydrogel. Therefore, an experimental model of the noncontact mechanical loading system based on magnetic force is put forward. By adding the magnetic ends with magnetic beads to hydrogel samples and combing with the finite element analysis, we optimize the strength and gradient of the external magnetic field to achieve the test for the mechanical properties of gel samples. The testing system overcomes the technical bottlenecks of traditional mechanical testing methods, such as difficult loading of hydrogel and easy destruction of samples.

According to time, the interaction between mechanical stimulation signals and cells in the microenvironment can be divided into three stages: mechanical transmission stage, receptive stage, and response stage. In the stage of mechanical transmission, the cells contact with the matrix and, thus, form adhesion plaque locally. And then, we can start a series of downstream signal pathways to achieve the collection and assembly of actin and tubulin in cells, forming a skeleton structure including the vascular and tubulin. The mechanical signals in cells will be transmitted along the microfilament. In the region close to the adhesion plaque, the intracellular filaments are often dense and intertwined to form strong stress fibers, which has a more stable combination with the extracellular matrix. In the receptive stage, the connection between the adhesion plaque and the cytoskeleton plays an important role. After the cells anchor the matrix and feel the external force stimulation, the response to the outside world is the mechanical response period.

Matrix materials are directly in contact with cells, and they participate in the formation of adhesion plaque, the assembly and dissociation of actin, the formation of pseudopodia, and other key physiological processes. The adjustability of mechanical properties is very important. According to different research purposes, the matrix materials are different. For example, the stiffness of extracellular matrix around different cells is different, and the stiffness of adult bone tissue can reach megapascal, or even gigapascal. To study the mechanical conduction behavior of bone cells, it is necessary to select matrix materials with high stiffness, such as glass, silicon, rubber, PMMA, and PDMS. When researching the response mechanism of soft tissue cells to extracellular matrix, it is necessary

to select matrix materials with lesser stiffness, such as hydrogel and polymer scaffolds.

According to the different matrix materials, it can be divided into inorganic nonmetallic materials and polymer materials. In any case, the matrix materials should have several characteristics, such as surface active molecules, hydrophilicity, and hydrophobicity. The matrix should be conducive to cell adhesion. Based on special technology, the active molecular array is modified on the surface of matrix to control the cell adhesion orderly. These methods mainly include PDMS stamping method, photo-assisted patterning method, and microfluidic-assisted patterning method. PDMS stamping method is mainly used to prepare PDMS stamp with different microarrays by Wiener technology, and modifies the active protein on the surface of microarray, then presses PDMS stamp on the surface of the matrix material. In addition, it modifies the active protein on the surface of matrix, the cells inoculated on the matrix only adhere to the position of active protein, thus forming an orderly cell array. The photo-assisted patterning method is mainly to graft photosensitive groups on active protein, and modify the ordered protein array on substrate through the photomask with special array. The microfluidic-assisted patterning method is to design a microchannel chip with mutual transmission. Each channel will flow to a coolant reservoir, and the active protein solution is filled in channels, so that the array is formed. The matrix material should have good mechanical properties (stiffness or viscoelasticity) and a large range of mechanical control. For rigid materials such as glass, silicon, rubber, and plexiglass, their stiffness is usually at the level of gigapascal, which is suitable for the construction of microenvironment of hard tissue (bone, cartilage). Hydrogels have good water-retaining property and mechanical adjustability, so they are applied in the construction of microenvironment of soft tissues (muscles and nerves).

The mechanical stimulation signals in microenvironment are mainly transmitted to cells through extracellular matrix, so the in-vitro simulation method is mainly to explore the response of cells by applying mechanical loads (such as tensile force, compressive force, and fluid shear force) to matrix materials. At present, there are two main mechanical loading methods. The first class is mainly aimed at the mechanical loading of single cell or single molecule based on optical tweezers, magnetic tweezers, glass microtubules, microfluidic chips, molecular combs, atomic force microscopy, and other loading platforms. For example, the optical tweezers is a single beam gradient force optical trap, which can load, control, and capture the single molecules at the micro–nano level. The atomic force microscope uses the microcantilever to sense and amplify the force between the tapered probe on cantilever and the sample atoms to achieve the detection. For example, Lim *et al.* used atomic force microscopy to research the elastic modulus of early cells and cancer cells of benign mammary tumors, respectively, and found that the elastic modulus of cancer cells is smaller, which is related to their migration ability. Maxim E. Dokukin *et al.* used the atomic force microscope probe to exert mechanical stimulation on epithelial cells and to research the adhesion behavior of cells on substrate under different strain conditions.

The characterization methods of cell mechanics microenvironment can be divided into the shown categories.

4.1 Characterization of matrix mechanical property

The characterization system of cell mechanical microenvironment mainly includes the characterization for the mechanical properties of matrix materials, cell mechanical behavior, and mechanical property of cell matrix interface. The mechanical properties of matrix mainly include stiffness and viscoelasticity. The stiffness of matrix can be tested by the traditional mechanical property detection method, micro–nano indentation instrument, and atomic force microscope. In the range of elastic deformation, Young's modulus is measured. Due to high water-retaining property of hydrogel matrix, its viscoelasticity is between Hooker elastomer and Newton fluid.

4.2 Characterization of mechanical behavior of cells

The traditional methods mainly focus on the matrix material but ignore the cell tension and the interface mechanics of cell and extracellular matrix. At present, elastic microcolumn confinement and tension microscope are the main methods to characterize the cell tension. The elastic microcolumn confinement method is mainly to use the micro–nano fabrication technology to prepare two-dimensional substrate with PDMS microcolumn array and modify the active protein, which is conducive to cell adhesion on the surface of microcolumn. The stiffness of microcolumn array can be controlled by changing the diameter or height of microcolumn.

4.3 Mechanical characterization of cell–matrix interface

The above characterization methods can test the mechanical properties of matrix materials or cells, but all of them are at the level of single cell, which are difficult to achieve the mechanical test at the molecular level, such as the connection strength of integrins and matrix protein, and the tensile strength of force sensitive protein on cell membrane. These mechanical properties are significant to research the cell mechanical conduction. At present, the main method to characterize the mechanical properties of cell matrix interface at the molecular level is the fluorescence tension probe method based on the principle of fluorescence resonance energy transfer. The gene cloning technology is used to insert the fluorescent probe into structural proteins of cells. Finally, the change of structural mechanics of cells are estimated quantitatively or semi-quantitatively by the fluorescent donor and receptor.

5 Conclusion

In this study, the method of machine vision is applied to the construction and research of cell mechanics microenvironment. When constructing the 3D cellular mechanical microenvironment, hydrogel stiffness, stress–strain stimulation, density of cell adhesion locus, and gel pore structure are usually coupled. The above factors are independently controlled by designing hydrogel cross-linking method and analyzed as a single factor. NIH/3T3 mouse fibroblasts are inoculated and cultured in the microgel column of gelatin methacrylate to achieve the separate regulation for gel stiffness, density of cell adhesion locus, and gel pore structure, which provide a powerful tool for the construction of 3D stiffness microenvironment. Experimental result show that the degradation of extracellular matrix is unable to affect the stiffness of gel within 5 days, and the increase in the stiffness of the hydrogel matrix helps to promote cell proliferation to a certain extent.

Funding information: This work was supported in part by the National Natural Science Foundation of China under Grant 92159102, Grant 11862006, Grant 61862025, in part by the Jiangxi Provincial Natural Science Foundation under Grant 20202BAB205011.

Author contributions: All authors have accepted responsibility for the entire content of this manuscript and approved its submission.

Conflict of interest: The authors state no conflict of interest.

Data availability statement: All data generated or analysed during this study are included in this published article.

References

[1] Shi J, Chen W, Wang Y. Evaluation research of communication and communication electronic warfare training efficiency under complex electromagnetic environment. J China Acad Electron Inf Technol. 2017;12(6):626–31.
[2] Yang G, Xiao F, Fan X. Hybrid modeling and control for three-level DC-DC converter. J Power Supply. 2018;16(3):1–8.
[3] Pei Y, Dou Y, Zhao J. Charge and discharge performance of lead-acid battery at low temperature in Antarctica, Chinese. J Power Sources. 2018;42(6):871–3+921.
[4] Chen Y, Huang J, Zhang J. Research on automatic batch deployment of virtual servers in IDC operating environment of large power enterprises. Autom & Instrum. 2017;8:99–101.
[5] Xiao X, Li J, Hu M. Crystal structure and antitumor activity of a triphenyl organotin complex. J Jilin Univ (Sci Ed). 2019;57(4):973–8.
[6] Liu C, Bian D, Wang W. Submarine dynamic modeling and simulation based on small perturbation theory. Computer Simul. 2019;36(8):20–4.
[7] Çitil HG. Investigation of a fuzzy problem by the fuzzy Laplace transform. Appl Mathematics Nonlinear Sci. 2019;4(2):407–16.
[8] Baskonus H, Bulut H, Sulaiman T. New complex hyperbolic structures to the lonngren-wave equation by using sine-gordon expansion method. Appl Mathematics Nonlinear Sci. 2019;4(1):129–38.
[9] Wu W, Chen R, Jia H. Game theory modeling for vehicle-pedestrian interactions and simulation based on cellular automata. Int J Mod Phys C. 2019;30(1):1950025.
[10] Dewasurendra M, Vajravelu K. On the method of inverse mapping for solutions of coupled systems of nonlinear differential equations arising in nanofluid flow, heat and mass transfer. Appl Mathematics Nonlinear Sci. 2018;3:1–14.
[11] Lin J, Wang Y, Wei X, Kong S, Liu Z, Liu J, et al. Controllable antibacterial and bacterially anti-adhesive surface fabricated by a bio-inspired beetle-like macromolecule. Int J Biol Macromolecules. 2020;157:553–60.
[12] Zhang T, He X, Deng Y, Tsang DCW, Yuan H, Shen J, et al. Swine manure valorization for phosphorus and nitrogen recovery by catalytic–thermal hydrolysis and struvite crystallization. Sci Total Environ. 2020;729:138999.
[13] Pönisch W, Weber C, Juckeland G. Multiscale modeling of bacterial colonies: how pili mediate the dynamics of single cells and cellular aggregates. N J Phys. 2017;19(1):015003.

[14] Alexander N, Ozarkar S, Beningo K. Transient mechanical strain promotes the maturation of invadopodia and enhances cancer cell invasion in vitro. J Cell Sci. 2017;130(11):1965.
[15] Simos TE, Tsitouras C. Evolutionary derivation of runge–kutta pairs for addressing inhomogeneous linear problems. Numer Algorithms. 2021;87:511–25.
[16] Kovalnogov VN, Simos TE, Tsitouras C. Ninth-order, explicit, two-step methods for second-order inhomogeneous linear ivps. Math Methods Appl Sci. 2020;43(2020):4918–26.
[17] Hazenbiller O, Nasr S, Krawetz J. Effect of mechanical strain on the pluripotency of murine embryonic stem cells seeded in a collagen-i scaffold. J Orthopaedic Res. 2017;36(2):799–807.
[18] Nikhil D, Arezoo M. Modeling of active swimmer suspensions and their interactions with the environment. Soft Matter. 2017;13(36):6033.
[19] Young A, Ngiow S, Gao Y. A2AR adenosine signaling suppresses natural killer cell maturation in the tumor microenvironment. Cancer Res. 2018;78(4):1003.
[20] Sarah A, David P, Ariena K. Synergy between the KEAP1/NRF2 and PI3K pathways drives non-small-cell lung cancer with an altered immune microenvironment. Cell Metab. 2018;27(4):935.
[21] Kim H, Nicole L, Su C. Microphysiological systems as enabling tools for modeling complexity in the tumor microenvironment and accelerating cancer drug development. Adv Funct Mater. 2019;29(22):1807553.